Modelling of spatial infection spread through heterogeneous population: from lattice to PDE models

Arvin Vaziry,[1] T. Kolokolnikov,[1] and P. G. Kevrekidis[2]

[1] *Department of Mathematics and Statistics, Dalhousie University Halifax, Nova Scotia, B3H3J5, Canada*
[2] *Department of Mathematics and Statistics, University of Massachusetts, Amherst, Massachusetts 01003-4515 USA*

We present a simple model for the spread of an infection that incorporates spatial variability in population density. Starting from first principle considerations, we explore how a novel PDE with state-dependent diffusion can be obtained. This model exhibits higher infection rates in the areas of higher population density, a feature that we argue to be consistent with epidemiological observations. The model also exhibits an infection wave whose speed varies with population density. In addition, we demonstrate the possibility that an infection can "jump" (i.e., tunnel) across areas of low population density towards the areas of high population density. We briefly touch upon the data reported for coronavirus spread in the Canadian province of Nova Scotia as a case example with a number of qualitatively similar features as our model. Lastly, we propose a number of generalizations of the model towards future studies.

1. INTRODUCTION

In the era of coronavirus, the ongoing public discussion frequently refers to the reproduction number R_0, as a (simple) single-number diagnostic that captures the entire epidemic for a given country or region; for a summary of mathematical discussions of this diagnostic, we refer the interested reader to [1–3]. In reality, R_0 is a parameter which changes locally, a feature that has not only been realized during the COVID-19 pandemic (see, e.g., [4]), but indeed one that has been well-known for similar outbreaks of other diseases such as dengue [5]. For example, it is natural to expect that areas with high population density and/or limited public health measures are hit much harder than more rural areas, or regions with strict health controls (masking and distancing). This suggests the limited value of describing the entire population by a single reproduction number R_0. In light of such considerations, herein we are interested in modelling of how the spread of disease depends on local spatio-temporal circumstances. One of the key parameter affecting the disease spread is population density. Our aim is thus to develop a simple, potentially generalizable model which captures the effect of population density and local differences on overall epidemic spread.

At the heart of many epidemiology models and in the frame of this study as well, are the so-called compartmental models, consisting of various classes of individuals and their interactions. Among the many possibilities that have arisen not only in the context of COVID-19, but also earlier, we note the formulation of ODE models [6–9], statistical models [7, 10], stochastic models [11], agent-based models [12, 13], spatial network models [10, 14] and partial differential equation (PDE) models [15, 16]; see also [12, 17] for reviews. Some of these works turn out to have a very deep influence on public thinking and policy [8, 13].

The focus of the present work will be on spatially-distributed models exploring the evolution of the infection not only temporally but also spatially. Indeed, such models have a time-honored history, e.g., in the format of meta-population models [18] and have been extensively used in the context of COVID-19 [19]. Such models have been used for a diverse host of countries including China [20, 21] and Spain [22, 23], while a comparison of different models developed, e.g., for the US can be found in the so-called COVID-19 Forecast Hub[1]. On the other hand, there exist also models that develop a PDE perspective such as [24, 25], in addition to earlier work by the present authors such as [15, 16] (see also references within these works).

Our aim in the present work is to complement the above approaches by means of a first-principles look into the development of the interaction between the different agents as they move through the spatial domain (and interact with each other). In so doing, we will develop a nonlinear dynamical lattice based approach, which can then be taken to the continuum limit, to yield a systematic PDE model that can be more suitable towards the modeling of COVID-19, as well as of other infectious diseases. Indeed, rather than incorporating standard processes such as diffusion and advection into an ODE SIR-type model, this perspective retrieves a nonlinear variant of diffusion which seems to us to be more well-suited to such epidemic settings. Additionally, a key advantage of the present model is that it enables a variety of generalizations to account for effects of longer range interactions (and, of course, additional effects such as those, e.g., of age distribution of the pandemic impact). Such potential extensions will be highlighted along the way. It is also relevant to mention that both for reasons of concreteness, but also for practical ones related to the identifiability of the model [26] (which does not escape us as a central issue and a consistent source of concern about complex models), we opt within the present seed study to focus on the prototypical SIR-type

[1] The relevant website is `https://covid19forecasthub.org/doc/ensemble/`.

model. Generalizations to more detailed models with a higher number of compartments will be evident, including also in connection to earlier work of some of the authors [15, 27].

Our presentation will be structured as follows. In section 2, we will present the theoretical formulation of our model (and its potential extensions). In section 3, we will use it to explore invasion waves and their respective speed. In section 4, the onset of an infection outbreak will be examined. Finally, after briefly touching upon the case example of Nova Scotia in section 5, we conclude and present some future challenges in section 6.

2. THEORETICAL FORMULATION OF THE MODEL

We start with an agent based model, with the aim of deriving a cellular automata model from it, and then consider its continuum limit to obtain a PDE system. A similar procedure was used in [28] to derive a spatio-temporal model of spreading of illegal activity. We assume that individuals can get infected by going out of their home and traveling to new locations. However they don't just simply walk at random, or diffuse: after going out (e.g. say for shopping or work), they return to their original (base) location.

To model individual motion, we discretize the space into bins. For illustration (and although the procedure straightforwardly generalizes to higher dimensions), we assume a one-dimensional grid whose bins are indexed by $j = 1 \dots N$. Let S_j, I_j, R_j denote the population of susceptible, infected, and recovered in bin j. As with the standard SIR model, we assume that infection occurs with some probability β per day when a susceptible individual encounters an infected individual. A susceptible individual in bin j can get infected in two ways: they either get infected within its own bin (e.g. infection spreading through families at home); or they might go out of their home and get infected outside their bin (e.g., going to work, shopping, etc); then return back to their original location. For simplicity, assume that individuals travel only to neighbouring bins $j-1$ and $j+1$ for work/shopping, then return back home. We will see how to extend the model past this simplifying assumption afterwards. In addition, assume for now that only susceptible individuals can travel (we will deal with a more general case below). Let α denote this daily travel rate (so that αS_j susceptibles travel from j to $j+1$ and αS_j travel from j to $j-1$). Let ΔI_j denote new infections per day in bin j. With above assumptions, we obtain,

$$\Delta I_j = \beta \left(S_j - 2\alpha S_j\right) I_j + \beta\alpha S_j I_{j-1} + \beta\alpha S_j I_{j+1} \tag{2.1}$$

Here, $\beta \left(S_j - 2\alpha S_j\right) I_j$ represents the daily new infections that happen in bin j; whereas $\beta\alpha S_j I_{j\pm1}$ is the total number of new infections within bin j acquired by individuals going to work/shopping etc in the neighbouring bins, then returning home with an infection (due to the interaction of these susceptibles with the infected individuals in bins $j \pm 1$.

The corresponding SIR model on a lattice then reads,

$$S_j(t+1) = S_j - \Delta I_j; \quad I_j(t+1) = I_j + \Delta I_j - \gamma I_j, \quad R_j(t+1) = R_j + \gamma I_j.$$

We now consider the continuum limit of this model, in the limit of many bins. Let dx be the grid spacing, so that $I_j \approx I(x)$ where $x = jdx$. We then estimate

$$\beta \left(S_j - 2\alpha S_j\right) I_j + \beta\alpha S_j I_{j-1} + \beta\alpha S_j I_{j+1} \approx \beta SI + \beta \left(dx\right)^2 \alpha S I_{xx}.$$

and we estimate $S_j(t+1) - S_j(t) \approx S_t$ (up to a rescaling by the time discretization increment dt and similarly for I and R. The resulting equations become

$$S_t = -D\beta SI_{xx} - \beta SI, \quad I_t = D\beta SI_{xx} + \beta SI - \gamma I, \quad R_t = \gamma I \tag{2.2}$$

where

$$D = \left(dx\right)^2 \alpha. \tag{2.3}$$

Note that unlike many other PDE models [24, 25, 29, 30], the "diffusion" term depends explicitly on the susceptible population density $S(x,t)$. Moreover, the "diffusion" enters into equation for S with a *negative* sign, whereas it has a positive sign in the equation for I.

Next, consider a more realistic model, where both susceptible as well as (e.g., asymptomatic [19, 27]) infected individuals travel, with rates α_S and α_I, respectively.

Then (2.1) gets replaced with

$$\begin{aligned} \Delta I_j = {} & \beta \left(S_j - 2\alpha_S S_j\right) \left(I_j + \alpha_I \left(I_{j-1} + I_{j+1} - 2I_j\right)\right) \\ & + \beta\alpha_S S_j \left(I_{j-1} + \alpha_I \left(I_{j-2} + I_j - 2I_{j-1}\right)\right) \\ & + \beta\alpha_S S_j \left(I_{j+1} + \alpha_I \left(I_{j+2} + I_j - 2I_{j+1}\right)\right). \end{aligned} \tag{2.4}$$

The limiting procedure results in equations (2.2), but with $\alpha = \alpha_S + \alpha_I$. Hence, we expect this to be the prototypical PDE-type model within this class of compartmental systems.

The remainder of the paper is concerned with the study of continuum equations (2.2). Before we do so, it is relevant to add a word about the possibility that traveling does not solely occur to bin $j \pm 1$ with rate $\alpha \equiv \alpha_1$, but similarly to $j \pm 2$ with rate α_2 etc. Then, it is straightforward to show that the Laplacian term is replaced by a nonlocal term of the form $S(x) \int K(x-y)I(y)dy$, where the (decaying with distance) kernel K is proportional to the probability of traveling between locations of distance $|x-y|$. A straightforward Taylor expansion around the vanishing argument of the kernel can be used to see that the diffusivity D above is proportional to the second moment (i.e., the variance) of the above kernel. More specifically, assuming for simplicity an even (or more generally isotropic) kernel

$$\int K(x-y)I(y)dy = \int K(\xi)I(\xi+x)d\xi \approx (\int K(\xi)d\xi)I(x) + DI_{xx} + \dots \tag{2.5}$$

Accordingly, the first term renormalizes β, while the second one produces the diffusive approximation with $D = (1/2)\int K(\xi)\xi^2 d\xi$. We can thus see how such beyond nearest-neighbor terms can generalize the model, while falling back to it in the simplest diffusive correction level of approximation. It is also interesting to further perceive how anisotropic kernels may lead to directed (convective rather than diffusive) motion, although the latter possibility will not be pursued further here.

3. EXAMINATION OF AN INVASION WAVE

One of the main effects of introducing a spatial dimension, is that the infection typically propagates from its origin. When the movement is sufficiently slow, this propagation happens in a wave-like fashion. One of the, arguably, simplest settings exhibiting wave propagation is the context of KPP-Fisher equation, modelling propagation of invasive species inside a favorable medium (see, e.g., [31] for a review):

$$u_t = du_{xx} + ru - su^2. \tag{3.6}$$

The travelling-wave solution has the form $u(x,t) = U(x-ct)$ where U satisfies the corresponding co-traveling ordinary differential equation (ODE)

$$-cU' = dU'' + rU - sU^2.$$

We seek a wave propagating from left to right, so that $U(z) \to 0$ as $z \to +\infty$, and $U \to r/s$ as $z \to -\infty$. Following the relevant standard theory and linearizing at the front of the wave ($z \to +\infty$), we can seek a solution of the form

$$U(z) \sim \exp(-\lambda z), \text{ as } z \to +\infty$$

which yields a dispersion relationship between the speed c and the decay rate λ of the form

$$c = d\lambda + \frac{r}{\lambda}. \tag{3.7}$$

The minimum speed of propagation is obtained by minimizing (3.7) over all admissable decay rates $\lambda > 0$, which yields

$$c_{\min} = 2\sqrt{dr}. \tag{3.8}$$

Numerical experiments confirm that the speed of propagation approaches $c_{\min}$ for a wide range of initial conditions, so long as $u(x,0)$ decays "sufficiently fast" as $x \to \infty$. This is a well-known feature of the KPP-Fisher equations [31, 32]. Note that this speed only depends on linear terms in (3.6) (i.e, it is independent of the value of s). Now suppose that the parameters d, r are functions of space x. If they vary sufficiently slowly, we expect that the speed of propagation will still be well approximated by (3.8). This is the so-called adiabatic approximation. We now return to the SIR model of Eq. (2.2). At the front of the infection of wave, we estimate $S(x)$ by $S_0(x)$, where $S_0(x)$ is the corresponding initial condition. The implicit assumption here is that $I, R \ll S$ and hence maintaining $S \approx S_0$ is a reasonable approximation. Then, this leads to the effective linear PDE for $I(x,t)$:

$$I_t \sim D\beta S_0(x) I_{xx} + (\beta S_0(x) - \gamma) I. \tag{3.9}$$

Assuming that the motion is sufficiently slow ($D \ll O(1)$), we linearize at the front of the wave similarly to our discussion above for the KPP-Fisher equation, and obtain the following approximation for the speed of propagation,

$$c(x) \sim 2\sqrt{D\beta S_0(x)(\beta S_0(x) - \gamma)}. \tag{3.10}$$

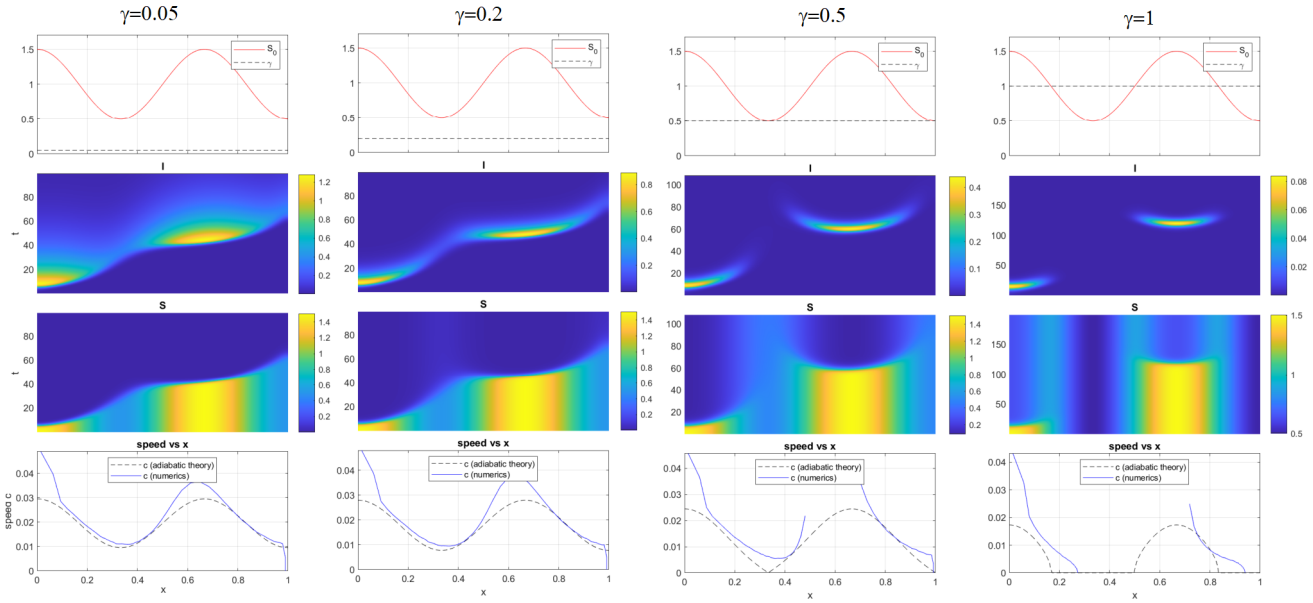

FIG. 1. Simulation of an infection wave propagating through a heterogeneous population, for several value of γ as indicated. Other parameters are: $\beta = 1$, $S_0(x) = 1 + 0.5\cos(3\pi x)$, $I_0(x) = 0.01\exp(-1000x)$, and $D = 0.0001$. The top row shows S_0 and γ. Areas where $\beta S_0(x) > \gamma$ (i.e. where red solid line is above the dashed line) are favorable for outbreak. The second row shows $I(x,t)$, the infection density propagating through the population. The third row shows $S(x,t)$, the density of susceptibles. The last row shows the speed c of the wave as a function of wave position x, comparing numerics to the adiabatic theory (see text). Note how the infection "tunnels" through areas of low infectivity in the last column. We used $N = 200$ meshpoints and $\Delta t = 0.001$. See Appendix for Matlab code to simulate (2.2).

Figure 1 shows a comparison between the formula (3.10) and full numerical simulations for several choices of γ. We used an implicit-explicit finite difference scheme to simulate the PDE of Eq. (2.2). As can be seen in the Figure 1, the adiabatic approximation (3.10) works relatively well in the areas where $\beta S_0(x) - \gamma > 0$. The formula breaks down in the areas where $\beta S_0(x) - \gamma \leq 0$. These areas can be thought of "buffer zones" where effective infection growth is negative; otherwise stated, the local R_0 is below unity and infection is suppressed therein. Nonetheless, the infection wave is able to "tunnel through" these areas, with some delay; see Section 5 for further investigation of this phenomenon.

4. THE ONSET OF THE OUTBREAK

Note that equations (2.2) admit a "trivial" solution corresponding to no outbreak; namely $I(x,t) = 0$ and $S(x,t) = S_0(x)$ where $S_0(x)$ describes the initial population distribution. We now explore the conditions for the initiation of the outbreak. At the onset of the outbreak, we may assume that $I(x,t) \ll 1$. Linearizing Eq. (2.2), in analogy to what is done for the ODE variant of the model to obtain the bifurcation associated with the spreading of the infection [1–3], leads to equation for I only of the form (3.9). Looking for solutions of the form $I(x,t) = e^{\lambda t}\phi(x)$, we obtain an eigenvalue problem

$$\frac{\lambda + \gamma}{\beta S_0(x)}\phi = D\phi_{xx} + \phi. \tag{4.11}$$

First, consider the limit $D = 0$. In this case, each point x in space evolves separately, and the eigenvalues λ are given by $\lambda \sim \beta S_0(x) - \gamma$. The outbreak is therefore prevented when $\beta S_0(x) < \gamma$ for all x, or $\gamma > \gamma_c$, where

$$\gamma_c = \beta \max_x S_0(x). \tag{4.12}$$

This can be thought of as a "spatially extended" generalization of the ODE result, in that the points in space are practically independent, hence for the epidemic to be suppressed, this needs to be achieved "individually" for every spatial point.

More generally, we define γ_c to be a threshold value of the decay parameter γ, corresponding to the zero-eigenvalue

of (4.11). Namely, γ_c satisfies

$$\frac{\gamma_c}{\beta S_0(x)}\phi = D\phi_{xx} + \phi; \tag{4.13}$$

the outbreak occurs if and only if $\gamma < \gamma_c$. For general $S_0(x)$ and D, the problem (4.13) does not have an explicit solution. However we expect γ_c to approach (4.12) as $D \to 0$. We now derive the corrections to (4.12) in the limit of small but non-zero D, i.e., for $0 < D \ll 1$ using asymptotic analysis. We expect the outbreak to first occur near the maximum of S_0. Let x_m be the point at which $S_0(x)$ has its maximum. As such, we expand:

$$x = x_m + \varepsilon y,$$

where ε is a small constant to be determined. Near x_m, write:

$$S_0(x) \sim A\left(1 - B\varepsilon^2 y^2\right) + O(\varepsilon^3), \quad \text{where } A = S_0(x_m); \quad AB = -S_0''(x_m)/2.$$

and we expand $1/S_0(x) \sim \left(1 + B\varepsilon^2 y^2\right)/A$. Problem (4.13) then becomes

$$\frac{\gamma_c}{A\beta}\left(1 + B\varepsilon^2 y^2\right)\phi \sim D\varepsilon^{-2}\phi_{yy} + \phi$$

We now choose ε so that $B\varepsilon^2 = D\varepsilon^{-2}$. In other words we let

$$\varepsilon := D^{1/4}B^{-1/4}.$$

Assuming ε is small, to leading order we obtain an eigenvalue problem

$$\phi_{yy} - y^2\phi = \mu\phi, \quad y \in \mathbb{R} \tag{4.14}$$

with

$$\mu = \left(\frac{\gamma_c}{A\beta} - 1\right) D^{-1/2}B^{-1/2}. \tag{4.15}$$

Equation (4.14) is a well-known quantum-harmonic oscillator eigenvalue problem whose eigenfunctions are given in terms of Hermite polynomials multiplied by a Gaussian. The corresponding eigenvalues are given by

$$\mu = 1, 3, 5, 7, \ldots$$

The smallest eigenvalue is $\mu = 1$. Setting $\mu = 1$ in (4.15) we obtain the following formula for the threshold value γ_c :

$$\frac{\gamma_c}{\beta} \sim S_0(x_m) - D^{1/2}\left(-S''(x_m)/2\right)^{1/2} S_0(x_m)^{1/2} + O(D). \tag{4.16}$$

For example, take $S_0(x) = a + \sin(\pi x)\,;\, \beta = 1, \quad x \in (0,1)$. Then the maximum occurs at $x_m = 0.5$ and we obtain

$$\gamma_c \sim 1 + a - D^{1/2}\pi\left(1 + a\right)^{1/2} 2^{-1/2} \tag{4.17}$$

The following table compares the formula (4.17) with the fully numerical solution of the eigenvalue problem (4.13), in the case of $a = 0$:

D	0.01	0.005	0.0025	0.00125
γ_c from numerics (4.13)	0.7686	0.8429	0.8889	0.9214
γ_c from asymptotics (4.17)	0.7778	0.8389	0.8871	0.9206
Relative error	1.18%	0.47%	0.20%	0.093%

The relative error appears to scale with a direct proportionality to D.

Let us also study the asymptotics in the limit of large D, on the domain $x \in [0, L]$ with Neumann boundary conditions $\phi(0) = \phi(L) = 0$. In this case, we expand ϕ in (4.13) as:

$$\phi = \phi_0 + \frac{1}{D}\phi_1 + \ldots$$

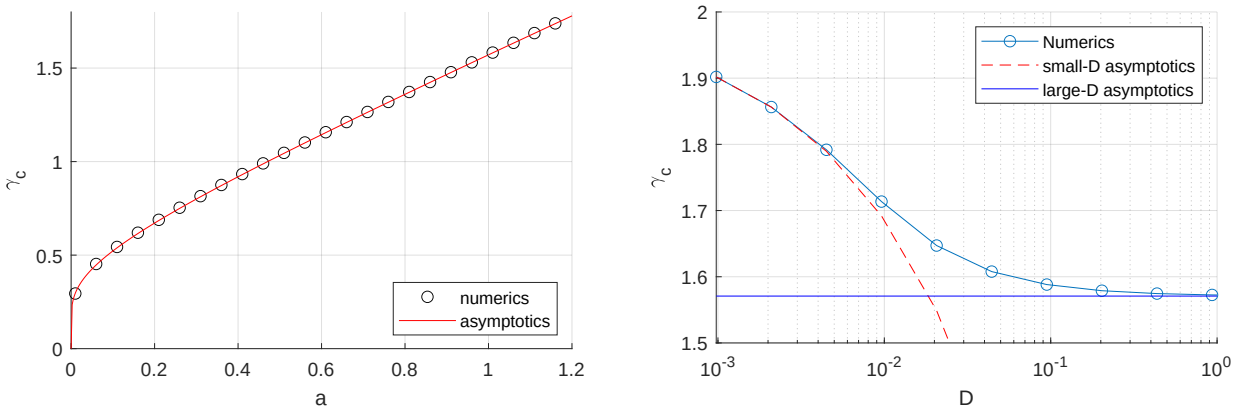

FIG. 2. Left: Threshold for outbreak γ_c in the limit of "large" D. Here, $D = 1$ and $S_0(x) = a + \sin(\pi x)$, $x \in (0, 1)$; $\beta = 1$. The numerical solution of (4.11) and asymptotics given by (4.20) are both shown. They are indistinguishable, with relative error less than 0.1%. Right: Threshold as a function of D with $S_0(x) = 1 + \sin(\pi x)$. Small and large-D asymptotics are also shown.

At leading order in D, we obtain $\phi_{0xx} = 0$. Together with boundary conditions $\phi'(0) = \phi'(L) = 0$, this yields $\phi_0(x) =$const. By scaling, we may then take $\phi_0 = 1$. The next-order equation for ϕ_1 then becomes

$$\frac{\gamma_c}{\beta S_0(x)} = \phi_{1xx} + 1. \tag{4.18}$$

We then integrate both sides from to obtain:

$$\gamma_c \sim \beta \left(\frac{1}{L} \int_0^L \frac{1}{S_0(x)} \right)^{-1}, \quad D \gg O(1) \tag{4.19}$$

The quantity $\left(\frac{1}{L} \int_0^L (S_0(x))^{-1} \right)^{-1}$ is called the harmonic average of $S_0(x)$.

For example, take $S_0(x) = a + \sin(\pi x)$ with $x \in (0, 1)$. Then (4.18) integrates to

$$\gamma_c \sim \begin{cases} \frac{\pi\sqrt{1-a^2}}{\log\left(1+\sqrt{1-a^2}\right)-\log\left(1-\sqrt{1-a^2}\right)}, & 0 < a < 1 \\ \pi/2, & a = 1 \\ \frac{\pi\sqrt{a^2-1}}{\pi - 2\arctan\left((a^2-1)^{-1/2}\right)}, & a > 1 \end{cases} \tag{4.20}$$

Figure 2(left) compares the asymptotics (4.20) with full numerical simulations of (4.13) for a wide range of a, and with $D = 1$. Despite a relatively small value of D, the agreement is excellent over the entire range of a (within 0.1%). On the right, we fix $a = 1$ and vary D; as can be seen, both large- and small- D asymptotics agree very well with full numerics. The intermediate regime of D, where neither of our approximations is value illustrates the most substantial deviations, yet we still have a very adequate description of the two asymptotic limits.

Finally, note that for constant population density S_0, the theshold γ_c defined by (4.13) is independent of D, and both (4.19) and (4.16) yield $\gamma_c = \beta S_0$. This may also be rather natural to expect as in that case, the diffusion term is "deactivated" and we are effectively back to the ODE problem case. One might naively expect that in the large-D limit, S_0 would be replaced by the arithmetic average of $S_0(x)$. However our analysis shows that the more appropriate formula is to take a *harmonic* average of $S_0(x)$ as in (4.19).

5. INDICATIVE OBSERVATIONS FROM COVID-19 IN NOVA SCOTIA AND "TUNNELING"

As a case study, consider the Canadian province of Nova Scotia where some of the authors of this paper reside. It has a population of about 1 million, with slightly less than half of those living in Halifax Regional Minicipality (HRM: the city of Halifax and surrounding area). The second-biggest town is Sydney (see map) with a population of 30,000. Much of the rest of the province has relatively low population density. Nova Scotia managed to completely suppress the initial outbreak in the spring of 2020 using very strict stay-at-home orders and border controls. Any visitor required a strict self-isolation quarantine of 2 weeks upon entry. As a result, there were very few locally-transmitted

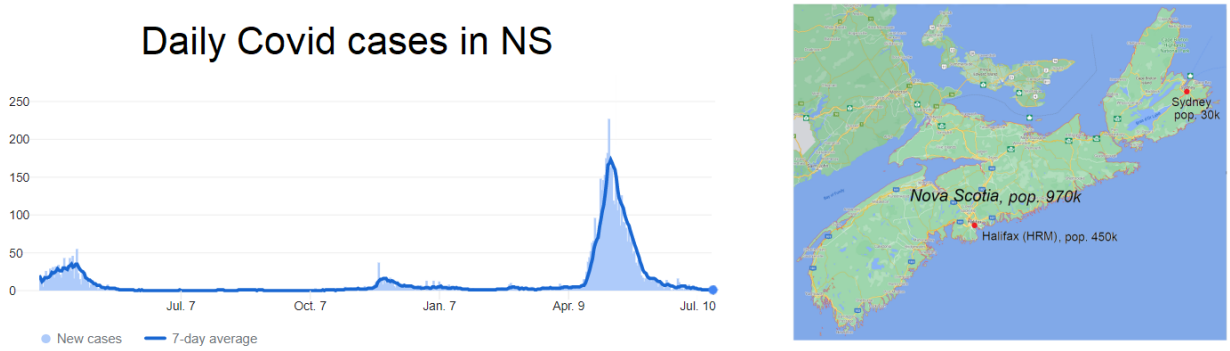

FIG. 3. Daily COVID-19 cases for the Province of Nova Scotia. Around 80% of the cases occurred in the Halifax Regional Minicipality, which contains about 50% of the population of Nova Scotia.

cases up until April 2021; stringent health measures managed to extinguish the few localized outbreaks that did occur before they spread.

Figure 3 shows the daily COVID case numbers for Nova Scotia. In total, as of July 2021, Nova Scotia had about 5800 cases, which is about 0.6% of the total population of 1 million. About 70% of these cases occurred during the "third wave" in April-June, 2021. Very few cases occurred in-between the three waves – and most of those were travel-related in quarantine (i.e., not involving community spread). Although less than half of NS population lives in HRM, it was responsible for 79% of the cases overall, and 81% of the cases in the third wave. Another 10.5% of cases occurred in Sydney, about 400km (4.5 hours drive) from Halifax, having a population of 30,000. Together, HRM and Sydney were responsible for over 90% of all infections, despite having about half of the overall population of the province. Despite its relatively smaller size, the infection rate in Sydney was about 2.5 times that of Halifax during the third wave.

The main takeaway lesson from this brief data summary, in connection to the qualitative model features discussed herein, is that the rate of infection is much higher in denser urban regions than the rest of Nova Scotia, which is mainly rural with low population density. This is indeed consistent with our model and its corresponding observations. In addition, due to stringent health measures, it is likely that the epidemic in most of the regions of Nova Scotia did not spread – even during the third peak – as almost all infections came from HRM and Sydney – the two biggest population centers in Nova Scotia. Despite strict travel restrictions (even inter-provincial travel was banned during the third wave in May 2021), the infection was able to "tunnel through" the rural areas from HRM to Sydney.[2]

Motivated by the above observations, we now show that our model can reporoduce, at least qualitatively, a "tunneling-through" effect, where the infection can spread between two regions of locally positive growth, even when separated by a "buffer zone" of negative growth (i.e., infection suppression). Consider a sample simulation as shown in Figure 4, with $S_0 = S_0(x) = 1.3 + \cos(2\pi x)$ with $x \in (0, 1.5)$ and $\beta = \gamma = 1$. Locally (in the limit of $D = 0$), the infection is suppressed in the middle region $x \in (0.298, 0.701)$ as well as for $x > 1.298$ where $S_0(x)\beta < \gamma$, and grows to the left and to the right of that region. We initially introduce the infection near the left boundary of $x = 0$. The outbreak then takes over the entre left region $0 \leq x \leq 0.298$ by the time $t = 20$. Then for a relatively long time $20 < t < 100$, nothing appears to happen. But eventually at around $t \approx 100$, the infection manages to "jump" over to the right region and re-appears at $x = 1$ (where $S_0(x)$ has its maximum), then spreads from there both to the left and to the right until the entire region $0.701 \leq x \leq 1.298$ is infected. It is interesting to note that when the infection re-appears at $t \approx 100$, it does so at $x = 1$ rather than $x \approx 0.7$. The reason merits further investigation, but roughly speaking, this happens because the local growth rate of infection is given roughly by $S_0(x)\beta - \gamma$, and is the highest at the maximum of $S_0(x)$. We remark that similar "jumps" of infection were investigated using network models in [33]. There, the authors investigated how network connectivity (and particularly, the presence of a few "long" edges connecting otherwise "local" regions) caused the appearence of new infection clusters. In [34], the authors also

[2] It is also interesting to note that there are other significant population centers closer to HRM that *did not* see anything near the size of outbreak in Sydney. This includes the towns of Truro (pop. 23000, one hour drive from Halifax) and New Glasgow (pop. 19000, 2 hours drive from Halifax) that did not see any significant outbreaks during the third wave. The outbreak in Sydney started with a hockey game, when kids and families from Halifax visited Syndey for a hockey tournament at the onset of the third wave, a potential superspreader event. At the end of the day, our simple model is insufficient to make predictions at such localized detail; much of the outbreaks are driven by random events and the luck of the draw, which our deterministic model is not designed in this first installment thereof to deal with. This is naturally an intriguing challenge for further work.

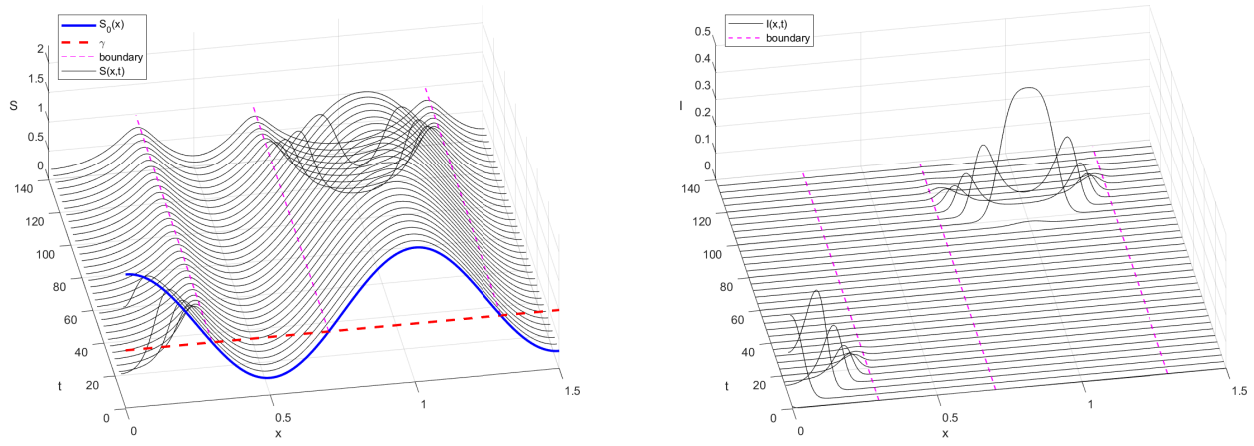

FIG. 4. Infection "tunneling" through a barrier. Initial conditions was taken to be $S_0(x) = 1.3 + \cos(2\pi x)$ with $\gamma = \beta = 1$ and $x \in [0, 1.5]$. Without spatial interactions ($D = 0$), the disease is suppressed in the middle region $x \in [0.298, 0.701]$ as well for $x > 1.298$. Here, we take $D = 0.00005$. The disease is introduced at $t = 0$ at the left end $x = 0$; corresponding to initial conditions $I(x, 0) = 0.001 \exp(-1000 * x)$. An infection wave propagating to the right is initially observed, but appears to die out around $t \approx 30$ as it hits the buffer region at $x \approx 0.3$. However it is able to "tunnel through" the buffer region, re-appearing at $x = 1$ (where S_0 has its maximum) when $t \approx 90$, then propagating from there to the rest of the infectious region $x \in [0.7, 1.3]$.

showed how tracking new clusters can be used to investigate the origin of the epidemic, and how network connectivity can predict the arrival times at various locations.

6. CONCLUSIONS AND FUTURE WORK

We have presented a model of spatio-temporal infection spread. We have started from a lattice variant of the problem and considered a first-principles inclusion of mobility according to which people move to new, adjacent locations (for work, shopping or other purposes), get infected and return to their base in that new infected state. The model allows for extensions whereby the mobility is to different locations (rather than to adjacent bins) with a presumably decaying over distance kernel. The latter constitutes an interesting variant of the current model relevant to examine in future work. Considering the continuum limit of the considered cellular automaton, we obtained a PDE (2.2) with state-dependent diffusion terms. Essentially, the scope of our work is to advocate the relevance of consideration of such terms, in addition to local ones and, arguably, instead of regular diffusion processes in this setting. The key assumption in our modelling is that while individuals move around, they don't diffuse, while infection does. While numerous PDE models exist in epidemiology (see, e.g., [15, 16, 24, 25, 29] for a sample), most assume either constant diffusion, or diffusion that is prescribed to be spatially-dependent. By contrast, we present a first-principles derivation of Eq. (2.2) from the underlying cellular automata representation of the basic infection mechanisms. Our model naturally leads to a diffusion that scales with the current number of susceptibles.

Introducing a spatial component to a basic SIR model spread also naturally explains why areas of high population density experience higher infection rates than more rural areas (for related approaches see e.g. [6, 35]). We also generalized the concept of the reproduction number in this spatially variable setting, by deriving an eigenvalue problem (4.11) whose solution describes overall decay or spread of the disease. Importantly, the relevant eigenvalue problem near the maximum of the susceptible population can be approximated by a quantum harmonic oscillator which allows an approximate analytical expression for the critical clearance rate that would avoid the spreading of infection. We have tested the relevant predictions numerically, finding very good agreement with our theoretical results, where appropriate.

Aside from spatially-dependent infection rates, our model demonstrates the difficulty of suppressing the outbreaks. As illustrated in Figure 4, the disease can "tunnel" between "islands" of positive growth separated by areas of negative growth (i.e., decay) of the epidemic. A better understanding and more systematic quantification of such phenomena is planned for future work.

There are also numerous additional dimensions in which the present consideration can be extended (both literally and figuratively). Indeed, here we restricted considerations to one-dimensional settings, i.e., "geographic corridors". In line with other works such as [15, 24], it is naturally more relevant to explore two-dimensional domains. In addition,

it is of substantial interest to consider infections across different age groups. Our considerations herein have assumed that the infectiousness and especially recovery properties of the entire population are the same, however it is well-understood that COVID-19 has a far more severe impact on more senior individuals with weakened immune system; indeed, this has been been the basis for designing relevant non-pharmaceutical intervention strategies [36]. It is then of interest to introduce kernels of interaction across a "synthetic dimension" representing age (in addition to spatial dimensions). There, interactions are predominant along the "diagonal" i.e., for people of the same age group, but there are nontrivial interactions between age groups at some "distance" between them (e.g., parents/grand-parents and children/grand-children); see, e.g., [37]. There, a more complicated non-monotonic kernel of interaction across ages may be relevant to include. These are all interesting possibilities, currently under consideration for future work and will be reported accordingly in future publications.

Appendix: Matlab code for model (2.2)

The following Matlab code was used to simulate (2.2). It uses implicit-explicit finite differences, where Laplacian is discretized impilcitly (for numerical stability, allowing for a relatively large time stepping) whereas nonlinear terms are handled explicitly. Cut-and-paste into Matlab to run.

```
N=200; x=linspace(0,1.5,N)';
I0=x*0; I0(1)=0.001;
S0=1.3+1*cos(x*pi*2);
D=0.00005; gamma=1; beta=1;

S=S0; I=I0;
dt=0.2; dx=x(2)-x(1);
Lap=-2*diag(ones(1,N))+diag(ones(1,N-1),1)+diag(ones(1,N-1),-1);
Lap(1,2)=2;Lap(N,N-1)=2; Lap=Lap/dx^2;
ID=eye(N); tnext=0;
Tsave=[]; Ssave=[]; Isave=[];

for t=0:dt:150
    L1=Lap*0;
    for i=1:N
        L1(i,:)=Lap(i,:)*S(i)*beta*D;
        L1(i,i)=L1(i,i)+S(i)*beta;
    end;

    B=ID*(1+dt*gamma)-dt*L1;
    Ihat=B\I;
    Shat=S-dt*L1*Ihat;
    I=Ihat; S=Shat;
    if t>tnext
        tnext=tnext+2;
        plot(x,S0+I0, '--r', x, gamma./beta+x*0, '--g',  ...
            x, (I), '-ok', x, S, '-b');
        title(sprintf('t=%g',t));
        drawnow;
    end;
    Ssave(:,end+1)=S; Isave(:,end+1)=I; Tsave(end+1)=t;
end;

%%
subplot(1,2,1); show_tx(Tsave,Isave, 0,1);
xlabel('x'); ylabel('t');title('I(x,t)');
subplot(1,2,2); show_tx(Tsave,Ssave, 0,1);
xlabel('x'); ylabel('t');title('S(x,t)');

function show_tx(T,U, a,b)
N = size(T,2); n = size(U,1);
x = linspace(a,b,n);
```

```
X = linspace(1,1,N)'*x;
Y = T'*linspace(1,1,n);
pcolor(X',Y',U);
shading('interp');
end
```

Acknowledgements. P.G.K. gratefully acknowledges support through the C3.ai Digital Transformation Institute and also enlightening discussions with the PEACoG group (M. Barmann, Q.-Y. Chen, J. Cuevas-Maraver, Y. Drossinos, G.A. Kevrekidis, Z. Rapti).

---

[1] N. Bailey, The mathematical theory of infectious diseases and its applications, Griffin, London, 1975.
[2] R. May, R. Anderson, Infectious diseases of humans: dynamics and control, Oxford University Press, Oxford, 1991.
[3] F. Brauer, C. Castillo-Chávez, Mathematical Models in Population Biology and Epidemiology, Springer-Verlag, New York, 2001.
[4] R. Thiede, N. Abdelatif, I. Fabris-Rotelli, R. Manjoo-Docra, J. Holloway, C. van Rensburg, P. Debba, N. Dudeni-Tlhone, Z. Kimmie, A. le Roux, Spatial variation in the basic reproduction number of covid-19: A systematic review, arXiv (2020) 2012.06301.
[5] T. Ng, T. Wen, Spatially adjusted time-varying reproductive numbers: Understanding the geographical expansion of urban dengue outbreaks, Sci. Rep. 9 (2019) 19172.
[6] H. Hu, K. Nigmatulina, P. Eckhoff, The scaling of contact rates with population density for the infectious disease models, Mathematical biosciences 244 (2) (2013) 125–134.
[7] A. L. Bertozzi, E. Franco, G. Mohler, M. B. Short, D. Sledge, The challenges of modeling and forecasting the spread of covid-19, arXiv preprint arXiv:2004.04741 (2020).
[8] S. M. Kissler, C. Tedijanto, E. Goldstein, Y. H. Grad, M. Lipsitch, Projecting the transmission dynamics of sars-cov-2 through the postpandemic period, Science 368 (6493) (2020) 860–868.
[9] L. Humphrey, E. W. Thommes, R. Fields, N. Hakim, A. Chit, M. G. Cojocaru, A path out of covid-19 quarantine: an analysis of policy scenarios, medRxiv (2020).
[10] Y. Xia, O. N. Bjørnstad, B. T. Grenfell, Measles metapopulation dynamics: a gravity model for epidemiological coupling and dynamics, The American Naturalist 164 (2) (2004) 267–281.
[11] D. Faranda, T. Alberti, Modeling the second wave of covid-19 infections in france and italy via a stochastic seir model, Chaos: An Interdisciplinary Journal of Nonlinear Science 30 (11) (2020) 111101. arXiv:https://doi.org/10.1063/5.0015943, doi:10.1063/5.0015943.
URL https://doi.org/10.1063/5.0015943
[12] H. McCallum, N. Barlow, J. Hone, How should pathogen transmission be modelled?, Trends in ecology & evolution 16 (6) (2001) 295–300.
[13] N. Ferguson, D. Laydon, G. Nedjati Gilani, N. Imai, K. Ainslie, M. Baguelin, S. Bhatia, A. Boonyasiri, Z. Cucunuba Perez, G. Cuomo-Dannenburg, et al., Report 9: Impact of non-pharmaceutical interventions (npis) to reduce covid19 mortality and healthcare demand (2020).
[14] V. Colizza, A. Vespignani, Epidemic modeling in metapopulation systems with heterogeneous coupling pattern: Theory and simulations, Journal of theoretical biology 251 (3) (2008) 450–467.
[15] P. G. Kevrekidis, J. Cuevas-Maraver, Y. Drossinos, Z. Rapti, G. A. Kevrekidis, Reaction-diffusion spatial modeling of covid-19: Greece and andalusia as case examples, Phys. Rev. E 104 (2021) 024412. doi:10.1103/PhysRevE.104.024412.
URL https://link.aps.org/doi/10.1103/PhysRevE.104.024412
[16] C. Gai, D. Iron, T. Kolokolnikov, Localized outbreaks in an sir model with diffusion, Journal of Mathematical Biology 80 (5) (2020) 1389–1411.
[17] D. Chen, Modeling the spread of infectious diseases: A review, in: Analyzing and modeling spatial and temporal dynamics of infectious diseases (2014) pp. 19–42.
[18] V. Colizza, A. Vespignani, Epidemic modeling in metapopulation systems with heterogeneous coupling pattern: Theory and simulations, Journal of Theoretical Biology 251 (3) (2008) 450–467. doi:https://doi.org/10.1016/j.jtbi.2007.11.028.
URL https://www.sciencedirect.com/science/article/pii/S0022519307005991
[19] D. Calvetti, A. P. Hoover, J. Rose, E. Somersalo, Metapopulation network models for understanding, predicting, and managing the coronavirus disease covid-19, Frontiers in Physics 8 (2020) 261. doi:10.3389/fphy.2020.00261.
URL https://www.frontiersin.org/article/10.3389/fphy.2020.00261
[20] J. Zhang, L. Dong, Y. Zhang, X. Chen, G. Yao, Z. Han, Investigating time, strength, and duration of measures in controlling the spread of covid-19 using a networked meta-population model, Nonlinear Dyn. 101 (2020) 1789–1800.
[21] R. Li, S. Pei, B. Chen, Y. Song, T. Zhang, Y. W., J. Shaman, Substantial undocumented infection facilitates the rapid dissemination of novel coronavirus (sars-cov-2), Science 368 (2020) 489–493.
[22] F. Aràndiga, A. Baeza, I. Cordero-Carrión, R. Donat, M. C. Martí, P. Mulet, D. F. Yáñez, A spatial-temporal model for the evolution of the covid-19 pandemic in spain including mobility, Mathematics 8 (10) (2020). doi:10.3390/math8101677.

URL https://www.mdpi.com/2227-7390/8/10/1677
[23] A. Arenas, W. Cota, J. Gómez-Gardeñes, S. Gómez, C. Granell, J. T. Matamalas, D. Soriano-Paños, B. Steinegger, Modeling the spatiotemporal epidemic spreading of covid-19 and the impact of mobility and social distancing interventions, Phys. Rev. X 10 (2020) 041055. doi:10.1103/PhysRevX.10.041055.
URL https://link.aps.org/doi/10.1103/PhysRevX.10.041055
[24] A. Viguerie, G. Lorenzo, F. Auricchio, D. Baroli, T. J. Hughes, A. Patton, A. Reali, T. E. Yankeelov, A. Veneziani, Simulating the spread of covid-19 via a spatially-resolved susceptible–exposed–infected–recovered–deceased (seird) model with heterogeneous diffusion, Applied Mathematics Letters 111 (2021) 106617.
[25] Y. Mammeri, A reaction-diffusion system to better comprehend the unlockdown: Application of seir-type model with diffusion to the spatial spread of covid-19 in france, Computational and Mathematical Biophysics 8 (1) (2020) 102–113. doi:doi:10.1515/cmb-2020-0104.
URL https://doi.org/10.1515/cmb-2020-0104
[26] V. K. Nguyen, F. Klawonn, R. Mikolajczyk, E. A. Hernandez-Vargas, Analysis of practical identifiability of a viral infection model, PLOS ONE 11 (12) (2016) 1–16. doi:10.1371/journal.pone.0167568.
URL https://doi.org/10.1371/journal.pone.0167568
[27] J. Cuevas-Maraver, P. Kevrekidis, Q. Chen, G. Kevrekidis, V. Villalobos-Daniel, Z. Rapti, Y. Drossinos, Lockdown measures and their impact on single- and two-age-structured epidemic model for the covid-19 outbreak in mexico, Mathematical Biosciences 336 (2021) 108590. doi:https://doi.org/10.1016/j.mbs.2021.108590.
URL https://www.sciencedirect.com/science/article/pii/S0025556421000390
[28] M. B. Short, M. R. D'orsogna, V. B. Pasour, G. E. Tita, P. J. Brantingham, A. L. Bertozzi, L. B. Chayes, A statistical model of criminal behavior, Mathematical Models and Methods in Applied Sciences 18 (supp01) (2008) 1249–1267.
[29] E. E. Holmes, M. A. Lewis, J. Banks, R. Veit, Partial differential equations in ecology: spatial interactions and population dynamics, Ecology 75 (1) (1994) 17–29.
[30] P. Kevrekidis, J. Cuevas-Maraver, Y. Drossinos, Z. Rapti, G. Kevrekidis, Spatial modeling of covid-19: Greece and andalusia as case examples, arXiv preprint arXiv:2005.04527 (2020).
[31] J. Xin, Front propagation in heterogeneous media, SIAM Review 42 (2000) 161–230.
[32] J. Murray, Mathematical Biology, Springer-Verlag, Heidelberg, 2002.
[33] D. Taylor, F. Klimm, H. A. Harrington, M. Kramár, K. Mischaikow, M. A. Porter, P. J. Mucha, Topological data analysis of contagion maps for examining spreading processes on networks, Nature communications 6 (1) (2015) 1–11.
[34] D. Brockmann, D. Helbing, The hidden geometry of complex, network-driven contagion phenomena, science 342 (6164) (2013) 1337–1342.
[35] T. Kolokolnikov, D. Iron, Law of mass action and saturation in sir model with application to coronavirus modelling, Infectious Disease Modelling 6 (2021) 91–97.
[36] A. Fokas, J. Cuevas-Maraver, P. Kevrekidis, Easing covid-19 lockdown measures while protecting the older restricts the deaths to the level of the full lockdown, Sci. Rep. 11 (2021) 5839. doi:10.1038/s41598-021-82932-8.
URL https://doi.org/10.1038/s41598-021-82932-8
[37] V. Ram, L. Schaposnik, A modified age-structured sir model for covid-19 type viruses, Sci. Rep. 11 (2021) 15194. doi:10.1038/s41598-021-94609-3.
URL https://doi.org/10.1038/s41598-021-94609-3